The Journal of Undergraduate Research in Physics

CONTENTS

VOLUME 9, NUMBER 1

OCTOBER, 1990

Published by the Physics Department of Guilford College
for
The American Institute of Physics and The Society of Physics Students

THE JOURNAL OF UNDERGRADUATE RESEARCH IN PHYSICS

This journal is devoted to research work done by undergraduate students in physics and its related fields. It is to be a vehicle for the exchange of ideas and information by undergraduate students. Information for students wishing to submit manuscripts for possible inclusion in the Journal follows.

ELIGIBILITY

The author must have performed all work reported in the paper as an undergraduate. The subject matter of the paper is open to any area of pure or applied physics or physics related field.

SPONSORSHIP

Each paper must be sponsored by a full-time faculty member of the department in which the research was done. A letter from the sponsor, certifying that the work was done by the author as an undergraduate and the the sponsor is willing to be acknowledged in the paper, must accompany the manuscript if it is to be considered for publication.

SUBMISSION

Two copies of the manuscript, the letter from the sponsor and a telephone number where the author can be reached should be sent to:

Dr. Rexford E. Adelberger, Editor
THE JOURNAL OF UNDERGRADUATE
RESEARCH IN PHYSICS
Physics Department
Guilford College
Greensboro, NC 27410

FORM

The manuscript should be typed, double spaced, on 8 1/2 x 11 inch sheets. Margins of about 1.5 inches should be left on the top, sides, and bottom of each page. Papers should be limited to fifteen pages of text in addition to an abstract (not to exceed 250 words) and appropriate drawings, pictures, and tables. Manuscripts may be submitted on a disk that can be read by a MacIntosh™. The files must be compatible with MacWrite™ or MicroSoft Word™. Illustrations should be in a MacDraw™ or MacPaint™ PICT format.

ILLUSTRATIONS

Line drawings should be made with black ink on plain white paper. Each figure or table must be on a separate sheet. Photographs must have a high gloss finish.

CAPTIONS

A brief caption should be provided for each illustration or table, but it should not be part of the figure. The captions should be listed together at the end of the manuscript

EQUATIONS

Equations should appear on separate lines, and may be written in black ink.

FOOTNOTES

Footnotes should be typed, double spaced and grouped together in sequence at the end of the manuscript.

SUBSCRIPTION INFORMATION

The Journal is published bianually, with issue one appearing in October and issue two in April of the next year. There are two issues per volume.

TYPE OF SUBSCRIBER	PRICE PER VOLUME
Individual	$US 5.00
Institution	$US 10.00

Foreign subscribers add $US 2.00 for surface postage, $US 10.00 for air freight.

To receive a subscription, send your name, address, and check made out to **The Journal of Undergraduate Research in Physics (JURP)** to the editorial office:

JURP
Physics Department
Guilford College
Greensboro, NC 27410

Back issues may be purchased by sending $US 15.00 per volume to the editorial office.

The *Journal of Undergraduate Research in Physics* is published by the Physics Department of Guilford College for the American Institute of Physics and the Society of Physics. **ISSN 0731-3764**

VOLUME 9 1990-91

The Journal of Undergraduate Research in Physics

Published by the Physics Department of Guilford College for

The American Insitute of Physics and The Society of Physics Students

ISSN 0731 - 3764

A GRADIENT INDEX OPTICS APPROACH TO ATMOSPHERIC REFRACTION

Robert P. Cunico
Department of Physics
Rochester Institute of Technology
Rochester, NY 14623

ABSTRACT

A numerical approach to the problem of atmospheric refraction was undertaken using the methods of Gradient Index Optics as an exercise in FORTRAN modeling. A model of the Earth's atmosphere was conceived to predict the apparent change in altitude of a point source due to refraction as observed at sea level. The model was able to predict the angular change in altitude to within 0.77% for rays with an observed elevation of greater than 5° and to within 11% for elevations between 1° and 5°. For lower elevations, the model deviated significantly from reality due to imprecision in the model of the atmospheric pressure gradient above 8×10^4 m.

INTRODUCTION

This paper is an exploration of computer modeling of physical phenomena, with the subject matter chosen to correspond to the author's personal interest. The Gradient Index approach of calculating the optical path in a complicated medium involves using a continuous or piecewise continuous function to represent a media's index of refraction. This method was chosen because of the novelty of the approach and the numerical analysis challenges it presented.

Theory

To determine the path s of a ray of light through a variable index of refraction n(s) it is appropriate to employ Fermat's principle: a light ray going from point s_o to s must form an optical path length L which is stationary with respect to variations of that path; $\delta L = 0$, where

$$L = \int_{s_o}^{s} n(s)\, ds \quad . \tag{1}$$

When considering a radially symmetric index of refraction n(r) and all rays coplanar with the origin of the refractive medium, it is sufficient to adopt a plane polar geometry. Using the Pythagorean theorem on an infinitesimal element of a typical ray as shown in Figure 1, one finds that

$$ds = (1 + r^2 \dot{\theta}^2)^{1/2}\, dr \quad . \tag{2}$$

where the dot represents differentiation with respect to r.

Substituting Equation 2 into Equation 1 gives the integral in terms of r and θ;

$$L = \int_{s_o}^{s} n(r)\ (1 + r^2 \dot{\theta}^2)^{1/2}\, dr \tag{3}$$

The conditions under which Equation 3 is stationary are found using Euler's theorem. Choosing r to be the independent variable with θ and $\dot{\theta}$ as the dependent variables gives the Euler equa-

---

Bob graduated in March of 1990 and is presently working at Kodak. He hopes to start graduate work in Optics in the Fall.

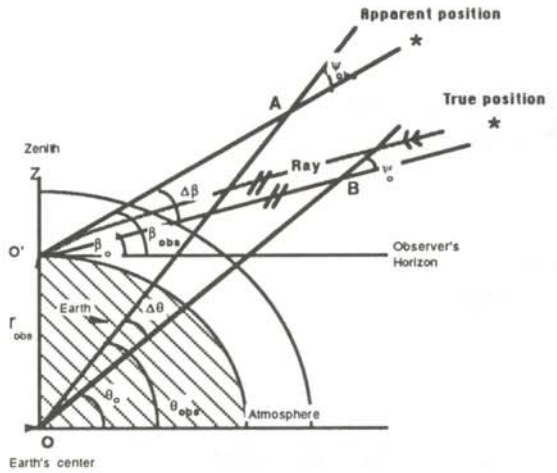

Figure 1.
Geometry of a light ray passing through the Earth's atmosphere. Light from a distant source impinges upon the upper atmosphere and is refracted through an angle $\Delta\beta$ to an observer at O'. The ray is initially parallel to the line O'B outside the atmosphere, but is bent gradually until it is parallel to the line O'A at O'.

tion for the integrand as

$$\frac{d}{dr}\frac{d}{d\dot{\theta}}\left[\, n(r)\ (1+r^2\dot{\theta}^2)^{1/2}\,\right] - \frac{d}{d\theta}\left[\, n(r)\ (1+r^2\dot{\theta}^2)^{1/2}\,\right] = 0\ , \tag{4}$$

which simplifies to

$$\frac{d}{dr}\left\{\, n(r)\, r^2\dot{\theta}\ (1+r^2\dot{\theta}^2)^{-1/2}\,\right\} = 0\ , \tag{5}$$

or

$$n(r)\, r^2\dot{\theta}\ (1+r^2\dot{\theta}^2)^{-1/2} = e\ , \tag{6}$$

where e is constant for all points along the actual path taken and therefore is assigned a value e. By solving Equation 6 for θ and substituting this into Equation 3, one obtains an expression for the change in elevation of the ray's tangent as it propagates from r_o to r as seen at O system in Figure 2;

$$\Delta\theta = e\int_{r_o}^{r}\frac{dr}{r\,[\,n^2(r)-e^2]^{1/2}}\ . \tag{7}$$

Examining Figure 1, one finds that Equation 6 can be greatly simplified by use of:

$$\sin\psi = r\frac{d\theta}{ds} = r\frac{\dot{\theta}}{\dot{s}} = r\,\dot{\theta}\,(1+r^2\dot{\theta}^2)^{1/2}\ . \tag{8}$$

Comparing the above with Equation 6 gives the more useful expression:

$$e = \pm\, n(r)\, r\sin\psi\ , \tag{9}$$

with e having the same sign as θ and where ψ is the angle between ds and dr. [1]

For light traversing the Earth's atmosphere from some infinitely distant source, $\Delta\theta$ represents the rotation of the ray tangent as seen at the Earth's center. The angle of elevation of the ray tangent $\beta(r)$ is given by:

$$\tan\beta(r) = \tan\theta(r) - \frac{r_{obs}}{r}\sec\theta(r)\ , \tag{10}$$

where r_{obs} is the radius to the intersection of the ray and the line OZ in Figure 2. Thus the angle ψ is just the difference between $\theta(r)$ and $\beta(r)$ for

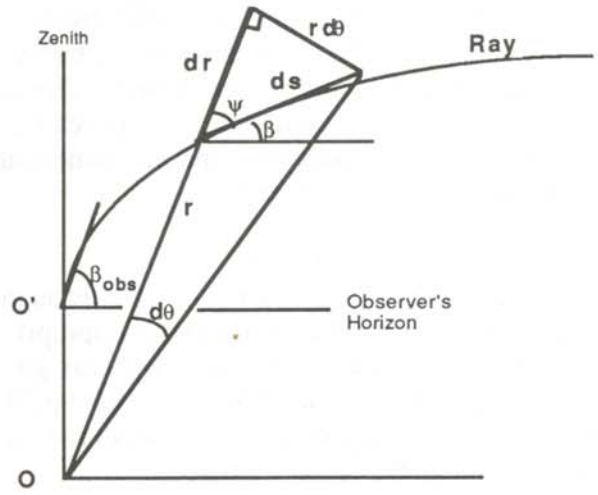

Figure 2
Detail of Figure 1, highlighting the geometry of a infinitesimal ray element.The angle subtended at O by an infinitesimal element of the ray's path ds, should not be confused with $\Delta\theta$ (not shown), the angle through which the ray is refracted as seen at O.

any point along the ray and $\beta(r_{obs})$ was the apparent elevation of the source at r_{obs} in the O' (observer's) system of Figure 2.

To find the change in elevation due to refraction $\Delta\beta$ as seen by an observer at O', one must find first find $\Delta\theta$ by integrating Equation 7, and then by employing Equation 9 at some known point, solve for $\Delta\beta$;

$$\begin{aligned}\Delta\beta &= \beta(r_{obs}) - \beta(r_o) \\ &= -[\theta(r_{obs}) - \beta(r_{obs})] + \delta\theta + \theta(r_o) - \beta(r_o) \\ &= -\psi + \delta\theta + \theta(r_o) - \beta(r_o) \\ &= -\sin^{-1}\left[\frac{\theta}{n(r_{obs})\, r_{obs}}\right] + \delta\theta + \theta(r_o) - \beta(r_o)\ ,\end{aligned} \tag{11}$$

where the subscripts 'o' and 'obs' denote values just outside the atmosphere and at the observer, respectively.

NUMERICAL METHOD

Because Equation 10 cannot be solved for $\theta(r)$ in terms $\beta(r)$ directly, determining $\Delta\beta$ for various incident angles $\beta(r_o)$ was done by choosing multiple values of $\theta(r_o)$ and solving for $\beta(r_o)$ instead. This was done far from the Earth's atmosphere where n(r) was assumed to be unity so that e can be easily computed. A functional form for n(r) was required to evaluate Equation 7 for $\Delta\theta$. This was found using readily available Chebyshev coefficients of the natural log of atmospheric pressure at altitude r_o, $p(r_o)$, and the relationship [2];

$$n(r) = n(r_o)\,\frac{p(r)}{p(r_o)} + 1 \tag{11}$$

Integration of Equation 7 was accomplished by first finding a Chebyshev series for the integrand, and then by manipulating the coefficients, a series for the integrand itself. Finally, $\Delta\beta$ was found by evaluating Equation 11. Any limits of integration could be used allowing refraction at heights other than sea level to be found so long as n(r) was known through that point.

In practice it was found that 50 terms were the maximum number that could be used in any of the series before machine round off error began to degrade accuracy.

The terms for the log pressure series were computed from a published Chebyshev series and tabulated data of actual pressures for the 1966 Standard Atmosphere model.[3] The use of both the series and data allowed increased accuracy over a much broader range than either alone could have provided; to an altitude of 10^6 m. The resultant series was accurate to 0.2% of the standard model below 8×10^4 m and to within 10% near 4×10^4 m degrading to 50% through 10^3 m. For observers near the earth's surface, the refraction above 10^6 m is not significant.

The construction, integration, and evaluation of all of the series were handled by 'public domain' software routines [4] which were found to be more than adequate for the task at hand. Briefly, the routines mapped and manipulated functions in the range [-1,1] over limits specified by the user [5]. The limits were slightly larger than required to avoid increased error between the series and its equivalent function near the end points of the function's range.

Because the tangent of angles very near $\pi/2$ were routinely required, quad precision was used throughout the program. Even for angles far from this limit, double precision computation was unacceptably inaccurate, and near the limit it was off by orders of magnitude.

Finally, it can be shown [6] that $\Delta\beta$ is approximately given by:

$$\Delta\beta = a\tan\beta(r_{obs}) - b\tan^3\beta(r_{obs})\ . \tag{12}$$

This approximation is valid for $\beta(r_{obs})>15°$, where a and b are empirically derived constants.[7] The constants a and b are, in practice, determined by the direct observation of standard stars at the observer's locale, and are strictly accurate only at that location. The constants are also weakly dependent upon wavelength.

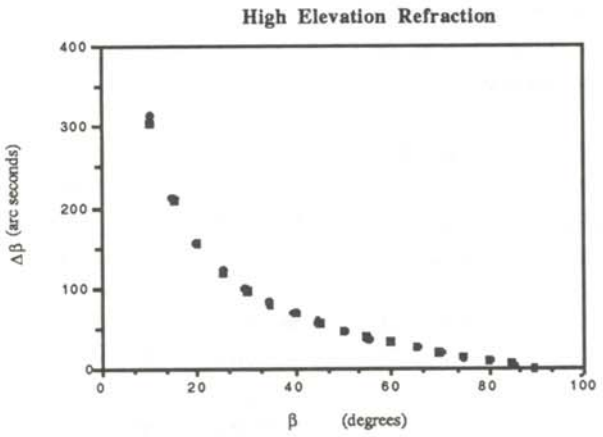

Figure 3
Refraction angle at high elevations. The diamonds are experimental data from reference 8. The squares are this work. The model shows no significant deviation from the observed seal level refraction $\Delta\beta$ above 1°.

RESULTS

The model was found to agree with the observed refraction at 550 nm [8] for most elevations as can be seen in Figures 3 and 4.. For β greater than 5°, the deviation from the accepted sea level values of refraction was 4.5", of the same order as short period variations in $\Delta\beta$ due to thermal currents in the troposphere. Below this angle, however, the model becomes increasingly inaccurate until at the horizon, β=-34', it is in error by 161". The disagreement between the predicted and the observed values for β>5° is, for all but the most stringent purposes, insignificant.

At all levels of the lower atmosphere, there are deviations from the model used. Such local factors such as wind, water vapor content, and temperature cause fluctuations in the pressure gradient over time scales from milliseconds to days which caused fluctuations in $\Delta\beta$ by as much as several arc-seconds. Thus, one can conclude that the model is accurate in this region.

However, for rays just skirting the horizon, a maximal path through all regions of the atmosphere is taken. Thus the any small errors in n(r) that are not significant at greater values of β causes much greater errors in $\Delta\beta$. This leads one to the known deviation of the pressure model at altitudes above $8x10^4$ m as the most obvious cause for the models failure near the horizon. The model's accuracy can be extended to all β by constructing a more accurate atmospheric pressure model and can be easily adapted to explore other atmospheres as well, provided the appropriate pressure gradient is known.

REFERENCES

1) E. Marchand, Gradient Index Optics, Academic Press, New York, 1978.

2) US Committee on Extension to the Standard Atmosphere 1964, US Standard Atmosphere Supplement1966, US Government Printing Office, Washington, DC (1966), p 72. Data used was for 45° Winter Supplementary Atmosphere.

3) Ibid.

4) Flannery, Press, Teukolsky, & Vetterling, Numerical Recipes, the Art of Scientific Computing, Cambridge University Press, NY; 1986. Routines CHEBFT, CHEBEV, CHINT pp 147-152. See legal agreement for use in the preface.

5) The domain of the function for which the series is to be found is mapped onto [-1,1], so the evaluation of any known function provides an experimental method of determining how large to make the initial domain. Over sizing by 10% was found to be sufficient.

6) R.M. Green, Spherical Astronomy, Cambridge University Press, New York, 1986, pp 87-95.

7) More terms for Equation 11 can be derived to extend the range to smaller β. However, the additional terms are heavily dependent on local conditions and are therefore of little use.

8) J. B. Sidgwich, Amateur Astronomer's Handbook, 4th ed. Enslow Publishers, Hillside, New Jersey, 1989, pp 444. Data are from the well known Pulkova tables. Similar tables are published in the current year's Astronomical Almanac ; US Government Printing Office, Washington, DC.

FACULTY SPONSOR

Dr John H. Campbell
Department of Physics
Rochester Institute of Technology
One Lomb Memorial Drive
Post Office Box 9887
Rochester, NY 14623-0887

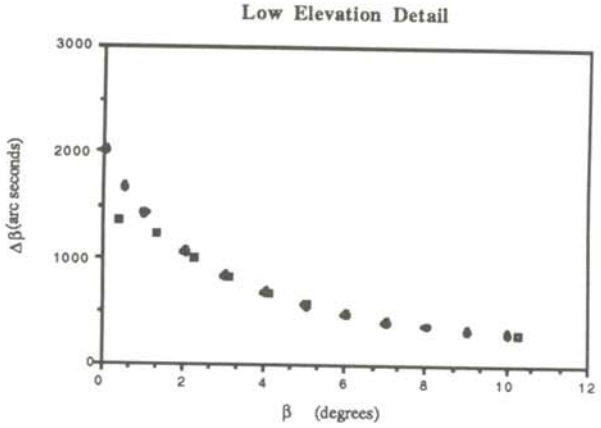

Figure 4
Refraction angle at low elevations. The diamonds are experimental data from reference 8. The squares are this work. The model shown no significant deviation from the observed sea level refraction $\Delta\beta$ above 1°. Below this, it rapidly deviates from the expected refraction.

AN APPARATUS FOR HYSTERESIS LOOP MEASUREMENT USING THE MAGNETO-OPTICAL KERR EFFECT

Robert Patrick Ridgeway
Department of Physics
Stetson University
Deland, FL 32720

ABSTRACT

The magneto-optical Kerr effect provides a means of investigating the magnetic properties of thin films. Thin ferromagnetic films are of current technological interest due to the role they play in magneto-optical recording. Information about the magnetic properties of these films can be obtained using the Kerr effect to generate hysteresis loops. The sample is placed between the poles of an electromagnet and the field swept while monitoring the polarization of the light reflected by the film. The magnetization of the film is determined by the rotation of the polarization of the reflected light. The apparatus for determining the hysteresis loop for a given thin film is described and a sample curve for a terbium-iron alloy is shown

INTRODUCTION

The magneto-optical Kerr effect (referred to as the Kerr effect in this paper) is one of the two phenomenon affecting the polarization of light that bears the name of John Kerr. [1] The Kerr effect is the change in the polarization of light reflected by a magnetized material due to its magnetization.

The Kerr effect can be observed in three distinct geometries, illustrated in Figure 1 [2]. The polar Kerr effect, which was used in this experiment, occurs when the applied magnetic field is perpendicular to the plane of the film. The longitudinal and transverse Kerr effects can be seen when the applied field is in the plane of the film. The effect can be studied by orienting the film and the applied field to observe any combination of the three.[3]

When linearly polarized light is reflected by a magnetized material in the polar geometry, it becomes elliptically polarized. However, if the incident light is polarized with the electric field component in the plane of incidence, the reflected light will still be linearly polarized, but the plane of polarization will be rotated.[4] The rotation that is caused by the polar Kerr effect, known as Kerr rotation, was found to be proportional to the magnetization of the sample under consideration [5] This makes it possible to generate a hysteresis loop, a plot of magnetization vs applied magnetic field, using the Kerr effect.

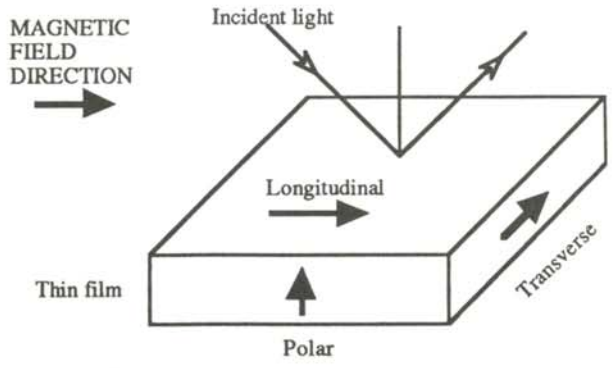

Figure 1
The three magneto-optical Kerr effect geometries: polar; longitudinal and transverse

Robert graduated from Stetson University in the spring of 1990. He is currently in the Nuclear Navy program and has recently graduated from officer candidate school.

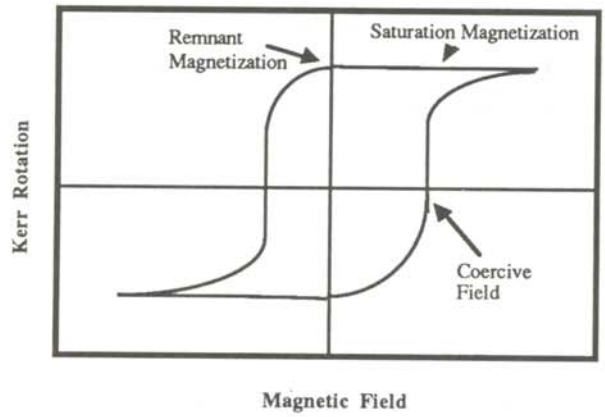

Figure 2
An example hysteresis loop generated using the Kerr effect that shows the coercive field, the remnant magnetization and the saturation magnetization.

The Kerr effect can be observed in light reflected by any ferromagnetic material. In this experiment we used a thin film of a rare-earth transition-metal (RETM) alloy, terbium-iron. The film is several monolayers of the RETM deposited on a reflective nonferromagnetic substrate. A RETM is an alloy which consists of a rare-earth element such as gadolinium, dysprosium or terbium and one or more of the transition elements such as cobalt, molybdenum or iron. [6] RETM films typically have large Kerr rotations.

Thin films of RETM are of interest for their use in magneto-optical recording, which has a possibility of replacing the magnetic recording material which is widely used today. [7] At this time one must still find a material that is not only stable with respect to time and oxidation, but also exhibits useful magneto-optical effects. The experiment described here is of the type that is used to determine the magneto-optical effects of the material: the coercive field and the remnant magnetization. The coercive field is the magnitude of the applied magnetic field that is necessary to observe the Kerr rotation and the remnant magnetization is the rotation of the polarization that would be observed under zero applied field. These features are shown in the example hysteresis loop shown in Figure 2.

THE EXPERIMENT

The apparatus used to generate the hysteresis loops was completely controlled by a microcomputer. A diagram of the experimental setup is shown in Figure 3.

The light from a 1 milliwatt helium-neon laser was 'chopped' by rotating a metal wheel with slits to give the beam a frequency of approximately 300 Hz. This frequency was monitored by the photoreflective sensor and used as the reference input for the lock-in amplifier. The light beam was then split by a half- silvered mirror such that half was directed into a "reference" phototube used to monitor any changes in the intensity of the laser. The rest of the light beam continued into the polarizer and struck the film that was placed between the poles of the electromagnet. The field strength of the magnet was monitored by the the microcomputer through the Hall effect Gauss meter.

The light that had its polarization rotated by the Kerr effect was analyzed using second analyzing polarizer. Malus' law states that the intensity of linearly polarized light passing through a two polarizers is proportional to the square of the co-

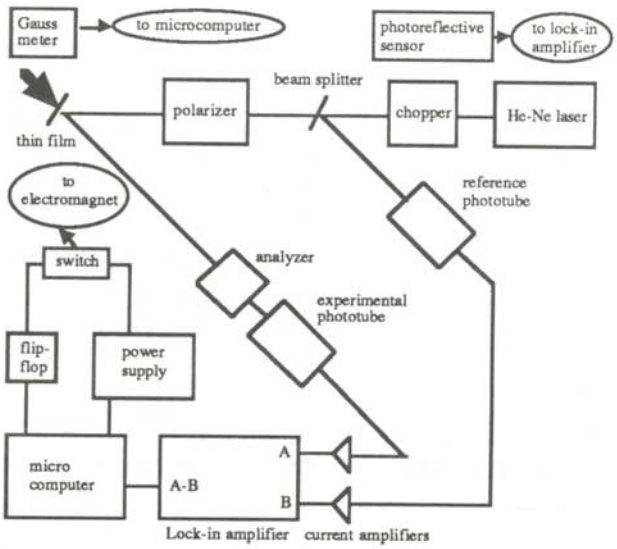

Figure 3
The experimental apparatus. The direction of the magnetic field is indicated by the solid arrow

sine of the angle between the two polarizers. [8] The intensity, and hence the rotation of the reflected light, was measured by a second phototube. The output of the first 'reference' phototube was subtracted from the output of the analyzing phototube by the lock-in amplifier to give a correct reading of the intensity change of light that leaves the analyzing polarizer.

The microcomputer maintained control over the apparatus by controlling the size and direction of the magnetic field. The 0 - 10 volt digital to analog output was fed into a voltage programmable power supply which provided the current for the electromagnet. The direction of the field could be changed by the computer by switching a logic level output and hence the polarity of the power supply.

The experiment was monitored by the microcomputer using the lock-in amplifier and the Gauss meter. A lock-in amplifier is a narrowband amplifier that can be used to filter out random signals. It was used to subtract the output of the two phototubes and then amplify this difference in the frequency range dictated by the photoreflective sensor. In this way, the large DC offset of the phototubes and any random noise caused by 60 Hz. 'pickup' from the power supplies was eliminated.

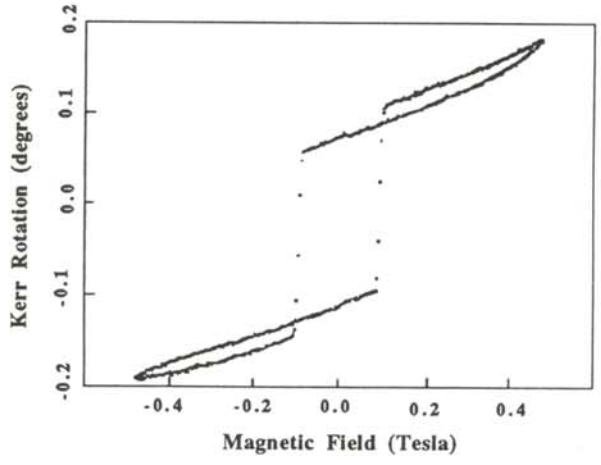

Figure 4
A signal averaged hysteresis loop for terbium-iron obtained using the polar Kerr effect

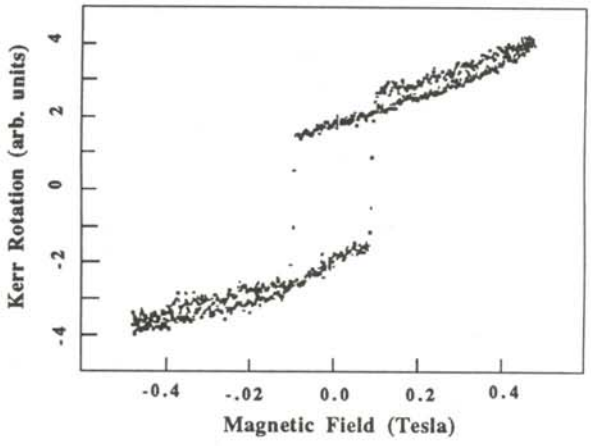

Figure 5
A hysteresis loop for the terbium-iron sample gernerated from one experimental trial.

The DC output of the lock-in amplifier, which was proportional to the Kerr rotation, was then stored as the y-axis value of a data point. The field strength, measured by the Gauss meter, was stored as the x-axis value for a data point.

DATA

The microcomputer was programmed to record data points as it changed the field in a linear manner from 0 to 0.50 T, back to 0.00 T, down to -0.50 T and back to 0 T. This was done 30 times. The data at each setting of the magnetic field were averaged to give the hysteresis loop shown in Figure 4. The ordinate of the graph was calibrated to degrees of rotation by monitoring the signal out of the lock-in amplifier when the analyzer was rotated under zero magnetic field.

Figure 4 shows that a 0.15 degree Kerr rotation was observed and that our sample had a coercive field of approximately 0.10 T. This is in agreement with data previously published on terbium-iron [9]. An uncalibrated hysteresis loop that was obtained from one trial is shown in Figure 5 to illustrate the improvement in the quality of the data when the signal is averaged over many loops.

The hysteresis loop shown in Figure 4 has two

interesting characteristics. The first is that the magnetization increases linearly as the applied field in increased instead of leveling off at some saturation magnetization as shown in Figure 2. The large slope can be attributed primarily to the paramagnetic properties of the glass substrate upon which the thin film was deposited. Paramagnetic substances exhibit induced magnetization that is proportional to the applied field.

The second intriguing quality of these data is the two additional loops (which have been observed in the literature [10]) that occur in the upper right and lower left of the hysteresis loop of Figure 4. One can see that the magnetization of the sample, observed through the Kerr rotation, is somewhat less as the magnetic field is being decreased than when it is being increased. It is believed that this results from the temperature of the film being raised by the joule heating in the electromagnet when the current is near its maximum. As the RETM film approaches its compensation temperature, the temperature at which the magnetization of the rare-earth and the transition-metal are equal and opposite, the net magnetization of the alloy goes to zero. [11] Since the alloy used had a compensation temperature that is just above room temperature, any additional heat supplied by the electromagnet results in a decrease in the net magnetization. This effect could be studied by controlling the temperature of the thin film to observe the Kerr rotation at different temperatures.

ACKNOWLEDGMENTS

The author would like to thank Dr. Kevin Riggs of Stetson University for his guidance and support during this project. He would also like to thank Dr. Thomas Lick and Deborah Freeborough for their assistance in writing and presenting this paper.

REFERENCES

1. J.M. Stone, Radiation and Optics, McGraw-Hill Book Company, Inc., New York, 1963, p. 447

2. L.E. Stover, "An Apparatus for Magneto-optic Studies", private communication.

3. J.M. Florczak, et. al., "Magnetication Processes of Epitaxial (100) Thin Fe Films Investigated by Kerr Magneto-Optical Effect", private communication.

4. S.R. Williams, Magnetic Phenomena, McGraw-Hill Book Company, Inc., New YHori, 1931, p. 169.

5. Ibid. p. 193.

6. S. Tsunashima, et. al., Journal of Applied Physics, 53, 1982, p. 8175.

7. M.S. Kryder, Journal of Applied Physics, 57, 1985, p. 3913.

8. J. Valasek, Introduction to Theoretical and Experimental Optics, John Wiley & Sons, Inc. New York, 1949, p. 193.

9. P. Wolniansky e. al., Journal of Applied Physics, 60, 1986, p. 348.

10. J.F. Dillon, Jr. et. al., Journal of Applied Physics, 64, 1988, p. 6099.

11. M. H. Kryder, Journal of Applied Physics, 57, 1985, p. 3915.

FACULTY SPONSOR

Dr. Kevin Riggs
Department of Physics
Stetson University
Deland, FL 32720

COMPUTER SIMULATION OF A NON-ZERO ELECTRON ANTINEUTRINO REST MASS

Shane D. Deichman
Department of Physics
University of California
Berkeley, CA 94720

ABSTRACT

Of the literal plethora of subatomic particles to enter the annals of science in the past fifty years, none is more enigmatic than the elusive "neutrino." In this paper, the author will examine the history surrounding this neutrally-charged lepton, including a presentation of the Fermi theory of beta decay, and outline some of the current efforts being made to measure the rest mass of the electron antineutrino. Finally, the cosmological consequence of a non-zero neutrino rest mass will be addressed.

INTRODUCTION

What is the ultimate fate of the Universe? Since the dawn of history, humans have pondered this question. The philosopher Aristotle, in his "Principle of Continuity," claimed that the Heavens were perfect and, therefore, unchanging. However, with the advent of contemporary scientific methodology, we have found that this isn't quite the case. Rather, our Universe exists in a state of continuous change. Modern experimental investigation has led us to believe that the Universe is expanding from a primordial fireball known as the "Big Bang." If this expansion will continue indefinitely or eventually collapse in a "Big Crunch" is a topic of intense debate.

One potential answer to this problem lies in an elusive particle known as the neutrino, meaning "little neutral one." Classified as a lepton, neutrinos invariably accompany beta-decay processes (with the possible exception of neutrinoless double-beta decay) and other weak subnuclear reactions, such as muon decay. After their initial hypothesis some fifty years ago, neutrinos have been assumed to be totally massless. Only recently has this aspect of modern physical theory been questioned. As it turns out, many of the new "Grand Unified Theories" (GUTs) call for the existence of massive neutrinos.

There are currently about twenty individual attempts to determine the rest mass of the electron antineutrino (the most common neutrino in our observations). The most recent estimates of the neutrino mass have placed upper limits of the order of 10 to 20 eV (electron volts) on this value.[1] For comparison, an electron has a mass of about 5.11×10^5 eV.

HISTORY AND THEORY

The neutrino was first postulated in 1930 by Wolfgang Pauli to account for both the missing spin factor of 1/2 and the unexpected electron energy spectrum of beta decay. A typical beta decay process is:

$$^{A}Z \rightarrow {}^{A}(Z+1) + e^{-} + \overline{\nu}_e$$

in which the energy spectrum of the beta particles is a continuum.The alpha decay energy spectrum, however, is composed of discrete peaks. The beta decay process would violate conservation of energy if there were not a third particle to take away the extra momentum and

Shane graduated from the University of California in 1989 and is now working in the Systems Analysis Group at the Naval Ocean systems Center in San Diego. He plans to pursue an interest in international security affairs.

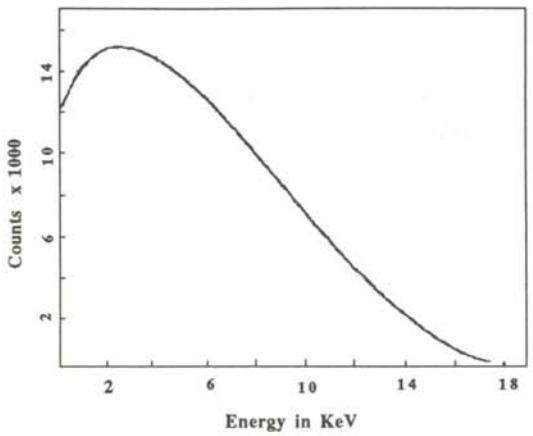

Figure 1
Beta Decay Spectrum for Tritium[4]

energy. This third body would also have to be elusive enough to evade prior detection. Interestingly, the neutrino was first known as the "neutron;" the particle we now know as the neutron wasn't discovered until a few years later.[2]

In 1934, Enrico Fermi published his famous theory of beta decay, of which the neutrino was an important part.[3] He pointed out that the rest mass of the neutrino would affect the energy spectrum of electrons emitted in beta decay, and gave the general form for the spectral shape in the absence of a neutrino mass.

The Fermi form for the probability of emitting an electron with total energy E is given by:

$$dN(E) = K\,|M|^2\,F(Z,R,E)\,p_e\,E\,(E_0-E)\,x\,[(E_0-E)^2 - m_\nu^2c^4]^{1/2}\,dE$$

where

$$K = G_F^2\,(m^5c^4/2\pi^3[h/(2\pi)]^7)\cos^2\theta_c,$$

M is the nuclear matrix element for the transition (for tritium, $|M|^2 \approx 5.55$), p_e is the electron momentum, E_0 is the end point energy (the maximum electron energy for a zero neutrino energy), m_ν is the neutrino mass, and F(Z,R,E) is a Coulomb correction factor that results from the effect of the nuclear charge on the wave function of the emitted electron. The shape of the beta decay function is shown in Figure 1.

In 1936, F.N.D. Kurie showed that the Fermi form for the beta spectrum could be linearized by plotting $[N(E)/E\,p_e\,F(Z,R,E)]^{1/2}$ vs. E.[5] This reparameterization allowed the effect of the neutrino mass to be seen much more clearly, as is shown in Figure 2. Furthermore, it allows the end point energy to be extrapolated from data taken at lower energies (where the count rates are higher), yielding a value which is independent of the neutrino mass. It turns out that the spectrum of tritium has an extremely straight Kurie plot due to the small impact of the nuclear effects. (The effects of spectrometer resolution and final-state distributions will be discussed later in this paper.)

In the "standard model," the neutrino is constrained to be completely left-handed (its spin pointing in the opposite direction of the motion) and to have zero mass. There is no compelling theoretical reason, however, for the mass to be zero; indeed, by analogy to the quark sector, one would expect $m_\nu \approx m_l$, where "l" is the lepton associated with a particular neutrino. In fact, for the electron and electron neutrino, $m_e/m_\nu > 10^4$. In general, though, grand unified theories (GUTs) predict non-zero neutrino masses. Therefore, the neutrino mass poses one of the most interesting unsolved problems in theoretical physics.[7]

One method of generating small neutrino masses is by the "see-saw" mechanism proposed by Murray Gell-Mann et al.[8] It requires that neutrinos be Majorana particles (i.e., that they be self-conjugate). Since the neutrino is electrically neutral, it could be its own antiparticle, assuming that it also has no magnetic moment, unlike the charged leptons which must be Dirac particles (i.e., having distinctive antiparticles). However, a Majorana mass for the neutrino implies that lepton number cannot be strictly conserved. In the "see-saw" scheme, a large mass term for right-handed neutrinos creates a small left-handed Majorana mass through a Dirac mass term which mixes the right- and left-handed fields, predicting lepton number violation.[9]

The question of whether neutrinos are Majorana or Dirac particles remains unsolved, though sev-

eral different experiments are sensitive to this question. For instance, the afore mentioned neutrino-less double-beta decay process can only occur if the neutrino is a massive Majorana particle.[10]

The impetus for the actual measurement of the neutrino mass came from some interesting experimental results. In 1980, there were several puzzling observations outstanding. The first was the measurement of the solar neutrino flux by Davis et al.[11] This flux has consistently come out to be about 1/3 the expected value from astrophysical calculations. The problem posed by this discrepancy has not yet been solved, though the effects of the sun's magnetic field on the kinematics of solar neutrinos (i.e., that the neutrino may have a non-zero magnetic moment, and may be therefore a Dirac particle) or neutrino oscillations[12] (in which a given neutrino oscillates in identity between the three known types or their antiparticles) are some possibilities. Also in 1980, Lyubimov et al. reported a positive neutrino mass in a tritium beta decay experiment at ITEP in Moscow utilizing tritiated valine.[13] This result was refuted by D.L. Wark at a recent conference in Tokyo.[14]

EXPERIMENTAL

Due to the incredibly low cross-section of neutrinos interacting with matter (on the order of 10^{-19} barns, or 10^{-43} cm^2!)[15], it is very difficult to measure neutrinos directly (they were not actually observed until nearly thirty years after their initial hypothesis). Therefore, one must use indirect methods to determine the neutrino mass. Perhaps the most popular of these methods is the precise examination of the beta-decay end point of tritium. Tritium is an ideal beta source in that it is reasonably active ($\tau_{1/2} \approx 12$ years.) and its spectrum is well known.

The experiment that sparked the current drive to determine the neutrino mass was initiated by V.A. Lyubimov of the Soviet ITEP in Moscow. His machine was a stainless-steel toroidal field beta spectrometer that was alleged to have had a very good resolution and high luminosity. By carefully studying the beta-decay end point of

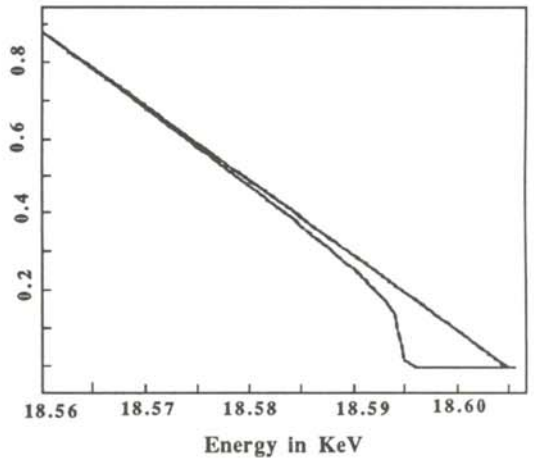

Figure 2
Kurie Plot for Tritium showing effect of 10 eV neutrino mass [6]

tritium and linearizing the decay curve, he hoped to learn the value of the neutrino mass.

Using a source of tritiated valine, placed at the first focus of the toroidal field spectrometer, Lyubimov claimed evidence for a non-zero neutrino mass of $14 \leq m_\nu \leq 46$ eV, with a best-fit value of 34 eV.[13] The experimental procedure was amplified in later papers, provoking a strong discussion. Much doubt has been cast on Lyubimov's results, primarily because of the difficulties incurred with solid, polyatomic molecular sources. The perturbative effects of the valine lattice and intramolecular forces create uncertainties on the order of 20 to 30 eV for the beta decay end point value, making it highly doubtful that accurate results could be obtained.[1]

An improvement on this method of observing the beta decay end point of tritium came in late 1980, when R.G.H. Robertson et al. at Los Alamos National Laboratory took the basic iron-free spectrometer design that Lyubimov had used and added a magnetic-field source tube containing gaseous molecular tritium. This elimination of the solid state and polyatomic perturbative effects attributable to solid molecular sources opened the door to significant improvements in end point resolution, and resulted in the first neutrino mass upper limit that was not dependent on the final atomic state configuration of

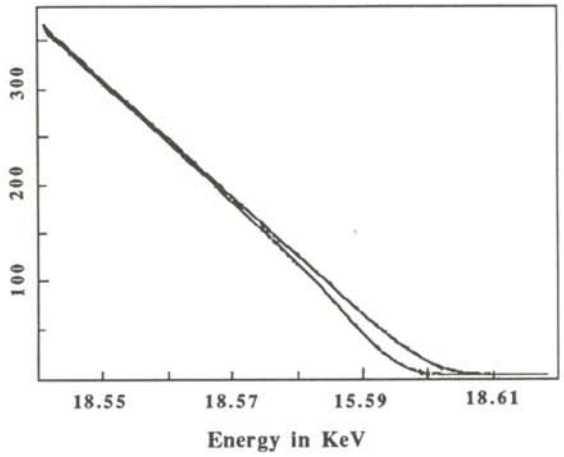

Figure 3
Convoluted Kurie Plot (resolution/FWHM ≈ 10 eV)[17]

the tritium (13.4 eV, 95% confidence level.).[14]

Many technical problems are encountered when one decides to use a gaseous radioactive source that needs to be circulated through a powerful magnetic field. For instance, one requires differential pumping mechanisms and other high vacuum apparati. However, the results are much more credible than those obtained using solid sources.

The next generation of the toroidal-field beta spectrometer came in 1984 at the Lawrence Livermore National Laboratory, where Wolfgang Stöffl improved the source tube of Robertson even more by inserting an RF dissociator into the apparatus. This resulted in the production of gaseous atomic tritium, which is ideal for highly precise measurements of the beta decay function.

The logic here is that tritium has the most well-understood beta decay curve of all known nuclides, and the final states distribution of the Helium-3 (the tritium beta decay daughter) is precisely known. Now, rather than having to contend with over 200 possible daughter states (as in molecular tritium), one can obtain more precise calculations by examining the far fewer excited daughter states of monatomic tritium. Before one can proceed further in determining the neutrino mass, a full understanding of the resolution function of one's spectrometer must be gained. Assuming a gaussian resolution function for a given spectrometer, the resolution is expressed as the FWHM (full-width at half-maximum) of the curve. This non-ideal resolving power represents itself as the convolution of a monochromatic source into a gaussian with the appropriate FWHM. For instance, suppose one had a source of 1 MeV gamma radiation and a detector array which had a resolution of 1 keV. The observed spectrum would then be a single Gaussian, FWHM = 1 keV, whose centroid is located at the channel corresponding to 1 MeV.

When observing a continuous spectrum with such a resolution, each discrete channel on that spectrum is essentially "smeared" into a gaussian with an appropriate FWHM. In order to "de-convolute" the observed spectrum so as to obtain the true distribution, one must have a deep understanding of the resolution function of the spectrometer.

Another perturbative effect mentioned above is the final states distribution. In the case of monatomic tritium, approximately 74% of the beta decays observed decay to the ground state of $^3He^+$, 25% decay to the first excited state (atomic), and so forth. There are no available nuclear excited states for the reaction.

This final states distribution manifests itself as a decrease in the intensity at high electron energies. Therefore, one must select a source which maximizes the intensity at these high energy levels so as to maintain a distinction between good events and background data or noise. Since 74% of tritium decays to the atomic ground state, tritium is again an ideal choice. Figure 3 shows a plot of the final observed spectrum, with the resolution function and final states distributions calculated into the Kurie plot from Figure 2.

The spectrometer being constructed at Livermore is expected to have a resolution of about 5 eV, which would yield unparalleled accuracy in the determination of the neutrino mass (or the determination of a new upper limit). This machine is being calibrated as of this printing, and should

begin taking actual data by early 1991.[18]

Some other experiments attempting to determine the neutrino mass use methods other than the one outlined above. For instance, de Rujula and Bennett proposed that the neutrino mass could be measured by observing the shape of the internal bremsstrahlung and x-ray spectrum following low Q-value electron capture.[19,20] Another method that has been proposed is the detection of neutrino oscillations, in which the experimenters look for the disappearance of one kind of neutrino or the appearance of another. This idea is not as general a test for neutrino mass as tritium beta decay or the internal bremsstrahlung methods mentioned above because it requires lepton number violation as well as massive neutrinos.

The only other significant type of experiment currently being used is the investigation of neutrino-less double beta decay, a process which can only occur if the neutrino is a massive Majorana particle (that is, its own antiparticle).[10] This method can be distinguished from two-neutrino double beta decay ($2\nu\ \beta\beta$ decay) by the energy spectrum of the beta particles. In $0\nu\ \beta\beta$ decay, the sum of the beta energies is constant, whereas the $2\nu\ \beta\beta$ decay spectrum is a continuum, so the former can be observed by detecting monoenergetic signals.

IMPLICATIONS

A tantalizing hint of physics beyond the "standard model" is evidenced by the "missing mass" problem in cosmology. This problem has been a topic of considerable interest in recent years.

The average density of the Universe can be characterized by the parameter $\Omega = \rho/\rho_C$, where ρ_C is the critical density required to "close" the Universe. This implies that, if $\Omega > 1$, the Universe is closed and will eventually collapse; if $\Omega < 1$, the Universe is "open" and will expand indefinitely; and if $\Omega = 1$, the Universe is "flat" and will expand forever, coming to rest at $t = \infty$.

The observed mass from spectroscopic analysis of galaxies gives an upper limit on the baryonic mass such that $\Omega_B < 0.1$.[21] Calculations of primordial nucleosynthesis provide an upper limit for the total possible baryonic density, claiming that $\Omega_B < 0.14 - 0.19$.[22] It is more appealing (both philosophically and aesthetically) to have Ω exactly equal to unity. Indeed, new "inflationary" theories of the early evolution of the Universe require that $\Omega = 1$.[23] If this is indeed the case, then 80-90% of the mass of the Universe is made up of non-baryonic matter. The neutrino is the only particle known to exist that could provide this mass. By virtue of the population of neutrinos in the Universe (one neutrino for every 1.7 photons, or about 10^{-8} nucleons per neutrino)[1], a neutrino mass as low as 15 eV could be sufficient to close the Universe. With the recent LANL upper limit of 13.4 eV, it would seem that the electron neutrino is not massive enough to close the Universe by itself. However, if the masses of all three neutrino types (e, μ, and τ) sum to greater than 45 eV (an average of more than 15 eV per neutrino), then neutrinos could still be the missing mass.

An early upper limit of 8 eV for closure was calculated by Cowsik and McClelland[24] based upon a value of 50 km sec^{-1} Mpc^{-1} for the Hubble constant and an assumption that there were two types of neutrinos, each of which had an antiparticle and two spin states. This limit seems too extreme when compared to more recent calculations, but it served to generate interest in neutrinos as possible contributors to the mass of the Universe.

Another aspect of the missing mass problem pertains to cluster dynamics and rotation curves of galaxies, indicating the presence of non-luminous halos surrounding them.[25] Neutrinos have been proposed as a candidate for this missing mass, though some argue that they are too energetic to be gravitationally bound.

SUMMARY

The determination of the neutrino mass is clearly one of the most provocative questions the scientific community now faces. With the advent of many Grand Unified Theories (GUTs) calling for the existence of massive neutrinos, it seems

that the time of massless neutrinos (as is needed by the "standard model") has come and gone.

If the neutrino is determined to have a positive mass, it will be the first experimental evidence of physics beyond the standard model. It could also lead to the resolution of a number of frustrating dilemmas which currently plague physicists (e.g., the "missing mass" problem in astrophysics).

Of the numerous attempts to measure the neutrino mass, one particular project at the Lawrence Livermore National Laboratory seems to defy the others in terms of expectations. Wolfgang Stöffl's spectrometer is expected to have a resolution of, and could be sensitive to, a neutrino mass of as little as 5 eV. If the neutrino mass is sufficient to "close" the Universe (i.e., $m_\nu \approx 15$ eV), it could be detectable by the summer of 1991.

REFERENCES

1 W. Stöffl, Lawrence Livermore Nat'l Lab; Prvt. Communication, 4/4/89.

2 R. Peierls, Contemp. Phys. 24, 221 (1983).

3 E. Fermi, Z. Phys. 88, 11 (1934).

4 D. Knapp, Dissertation presented to Princeton Physics Dept.; p. 8, (1986).

5 F.N.D. Kurie et al., Phys. Rev. 49, 368 (1936).

6 D. Knapp (op. cit.), p. 13.

7 S.P. Rosen, Lecture given at Moriond (1986)

8 M. Gell-Mann et al., Supergravity , North-Holland, Amsterdam, 1979).

9 E. Witten, Phys. Lett., 91B, 81 (1980).

10 E. Takasugi, Phys. Lett. 149B, 372 (1984).

11 J. Rowley et al., AIP Conf. Proc. #126; p. 1 (Homestake 1984).

12 F. Reines et al., Phys. Rev. Lett., 45, 1307 (1980).

13 V. Lyubimov et al., Phys. Lett., 94B, 266 (1980).

14 T.J. Bowles et al., XXIII Yamada Conference Proceedings on Nuclear Weak Process and Nuclear Structure; June 12-15, 1989.

15 K. Krane, Intro. Nuclear Physics (Wiley, New York, 1988); p. 296.

16 D. Knapp (op. cit.), p. i (Abstract).

17 LLNL Computer Analysis by S. Deichman, 7/88.

18 W. Stöffl et al., Nuclear Chem. Div. Annual Report/FY 87, (LLNL); p. 4-63.

19 A. de Rujula, Nucl. Phys., B188, 414 (1981).

20 C. Bennett et al., Princeton Nuclear Physics Proposal, 1980 (unpub.).

21 P. Frampton and P. Vogel, Phys. Rev., 82, 339 (1982).

22 J. Yang et al., Astrophys. Journal, 281, 493 (1984).

23 A.H. Guth, Phys. Rev., D23, 347 (1981).

24 R. Cowsik and J. McClelland, Phys. Rev. Lett., 29, 669 (1972).

25 V.C. Rubin, Science, 220, 1339 (1983).

FACULTY SPONSOR

Prof. Harry H. Bingham
Department of Physics
University of California
Berkeley, CA 94720
415-642-1920

PHASE DIAGRAM OF THE Na-As SYSTEM FOR 39.41-45.31 ATOMIC PERCENTAGE SODIUM *

John P. Sutter
State University of New York at Buffalo
Buffalo, NY 14261

ABSTRACT

Electromotive force (emf) was measured between 410C and 670C for an electrode containing a Na-As alloy with 45.31, 42 and 40 atomic percentage (at%) Na. These results were used to determine a partial phase diagram with an eutectic at 519.6C and 39.41 at% Na. Known phase diagrams of alloys of elements related to Na and As are compared to gather possible hints for the Na-As phase diagram. Emf measurements were also attempted over a 5 day period at 28.71 at%Na to test the effectiveness of this method at the As rich end. At the end of this time, the emf was still dropping.

INTRODUCTION

This paper describes the portion of the Na-As phase diagram from 39.41 to 45.31 atomic percentage (at%) Na at temperatures between 410 C and 670 C. Electromotive force (emf) measurements were taken from a cell whose working electrode contained a mixture of Na and As at 45.31, 42 and 40 at% Na. The liquidus lines determined from these data intersected at approximately 519.6 C and 39.41 at% Na, locating the eutectic temperature and composition. Emf measurements were also taken with another working electrode with 28.71 at% Na, but after 5 days, the cell still had not stabilized.

Some of the possible forms of the Na-As system come from potentiometric titration of a solution of Na in liquid NH_3 with a solution of As_2S_3 in liquid NH_3. Results of this show evidence for the formation of the species Na_3As, Na_3As_3, Na_3As_7 and $NaAs_5$ [1]. Unfortunately, the difficulties presented by the Na-As system have discouraged much earlier investigation. Not the least of these obstacles is the absence of a liquid phase for As at atmospheric pressure. (Gray As, the stable form at standard conditions, sublimates at 613 C.) This property makes the As rich compositions difficult to test with emf measurements.. The minimum amount of Na needed for producing good emf readings is not certain, but is taken here at about 38 at%. Furthermore, Ta, the usual material for leads in liquid metal electrodes, is vulnerable to attack by As vapors. Finally, the Na-As system approaches equilibrium sluggishly after titration. At the present time, no less than two or three days seem to be required for the cell to stabilize.

Despite the lack of literature on Na-As, one can form some guidelines for the behavior of this alloy from the phase diagrams of other alloys of alkali metals and Group 5A elements. K-As is the only alkali metal-As system that has a completely determined phase diagram. It shows a low K eutectic at 530 C and 41 at% K (very close to the eutectic we found for Na-As) [2]. Although the connections become less obvious if As is replaced with other Group 5A elements, the low Na eutectic appears at lower temperatures and proportions of Na as the period of the replacing element increases. Thus, Na-Sb has its low Na eutectic at 39.4 at% Na and 400 C. [3] The only known Na-Bi eutectic occurs at 21.8 at% Na and 218 C. [4].

John is a junior at the State University of New York at Buffalo majoring in physics. He collected data on the interactions of ^{28}Si nuclei prior to his stay at Argonne National Laboratory.

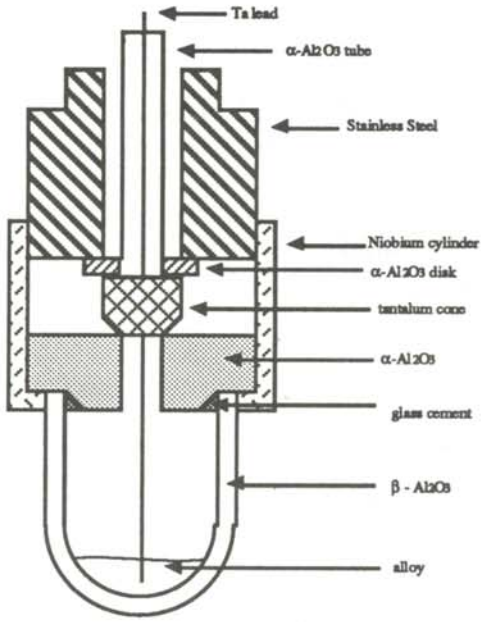

Figure 1
Schematic of the electrode assembly used for the working and reference electrodes.

The melting point peak of a 75 at% K alkali metal compound K-As is 655 C. [5] A similar melting peak at 856 C was found for Na-Sb and the melting point of Na_3Bi was found to be 775 C.[6] The first two peaks correspond to the formation of K_3As or Na_3Sb, which assume the hexagonal structure whose prototype is Na_3As. However, later emf measurements have placed the melting point of Na_3Bi at 848.1 C. [7]. The tentatively determined melting peak for Na-As is at 75 at% Na and approximately 750 C. Though counter to the melting point trend so far, it results from the formation of Na3As. However, the recent upward revision of the Na_3Bi melting point warns against taking this melting point value too seriously.

Compounds have been discovered at the equiatomic composition of all the complete phase diagrams mentioned, though they do not always cause melting peaks and seem to have fewer structural features in common. No information appears in the literature on the K-As structure except that its melting peak on the phase diagram is at 625 C. [5] NaSb, with a melting point of 465 C [6], also creates a melting peak and forms a 16-atom monoclinic unit cell [9]. NaBi, which has the Cu-Au structure [9], forms a peritectic at 446C and 53 at% Na [6]. These similarities may aid in deducing the phase diagrams of the Na-As system.

MATERIALS AND METHODS

Figure 1 shows the electrode assembly. The outer shell of both working and reference electrodes consists of a crucible of β-Al_2O_3, which is a solid electrolyte permitting current to pass through the electrode and an α-Al_2O_3 lid, joined to the crucible with a fired glass seal. Each electrode was placed in a high pressure helium glove box and filled with sample material through a hole in the lid. A Ta wire was then inserted into a Ta cone, which, in turn, was inserted into the electrode through the hole at the top. Finally, the Nb cylinder was slipped over the lid and cone and the stainless steel screw over the cover tightened to seal the electrode. The α-Al_2O_3 rings and tubes insulate the Nb cylinder and the screw from the Ta lead. Though the pure Na and the NaBi reference electrodes had Ta current collectors extending into the melt at the bottom, the Na-As electrode required a more corrosion resistant tungsten current collector.

Figure 2 shows the cell components. The working electrode is the Na-As electrode. The counter electrode bath, in which the working and reference electrodes are suspended, consists of approximately equal atomic fractions of Pb and Bi with about 10 at% Na. The bath was contained in a Mo crucible inside the glovebox and constantly stirred to reduce temperature and composition gradients. A Pt-Pt-10%Rh thermocouple immersed in the counter electrode bath

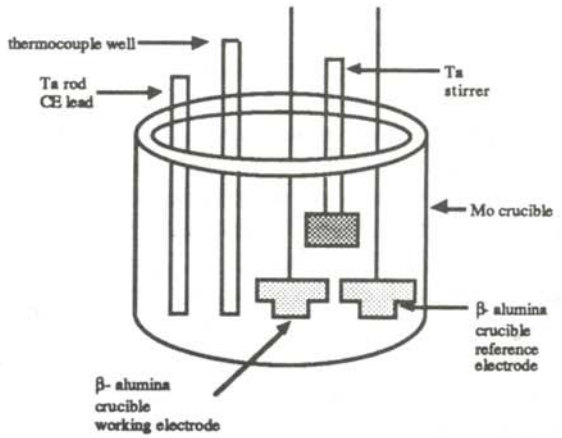

Figure 2
Diagram of the experimental apparatus.

measured the temperature. A digital coulometer allowed us to alter the working electrode composition by moving Na between the working electrode and the counter electrode bath. After each titration, the coulometer circuit was broken to allow the cell to reach equilibrium before any readings were taken.

In principle, the desired reference electrode is pure Na. However, a pure Na electrode would be impractical for the long periods at the high temperatures needed to bring Na-As into equilibrium. At the temperatures used here (412 C - 670 C), pure Na builds up high vapor pressure and appears to promote cracks in the β-alumina wall. As a result, a Na-Bi (15 at% Na) electrode was calibrated at lower temperatures (326 C - 491 C) against a pure Na electrode. The temperature dependence of the resulting emf was fit to a second degree polynomial. Once calibrated, this Na-Bi electrode became the secondary reference electrode for the Na-As system. At each desired composition, the emf between the Na-Bi and the Na-As electrodes was measured at various temperatures and added to the calibration emf.

RESULTS AND DISCUSSIONS

Figures 3-5 show the results of the emf measurements for 45.31, 42 and 40 at% Na. The results for 40 at% Na (Figure 5) proved difficult to reproduce because of metal deposits on the working electrode. They allowed undesirable titrating currents to pass through the electrode and change the composition of the working electrode. Because of this, the upturn in Figure 5 is

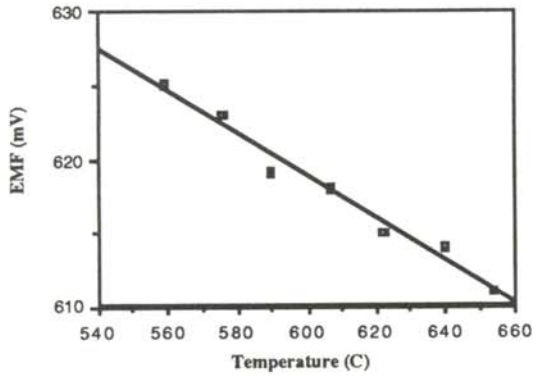

Figure 3
Emf vs temperature for $X_{Na} = 0.4531$.

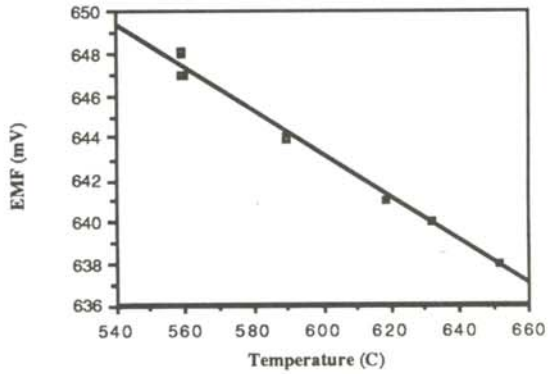

Figure 4
Emf vs temperature for $X_{Na} = 0.42$

almost certainly spurious.

The working electrode was replaced with a new one containing 28.71 at%Na, but the emf readings for the replacement electrode failed to stabilize. This instability may have been due to vaporization of As, which would have increased the atomic fraction of Na in the remaining melt and hastened corrosion of the interior working lead. During the subsequent attempt to titrate back to 42 at% Na at 400 mA (as a check on the new working electrode's accuracy), the circuit overloaded and the composition became uncertain.

The next attempt to titrate Na into the working electrode had to be done at a very high temperature (700 C) and very low currents. After 5 days, the resistance dropped suddenly, permitting a current of 300 mA without overload. However, even after a total of 380 Coul. had

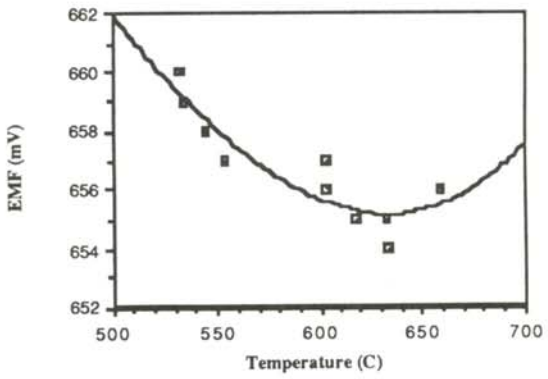

Figure 5
Emf vs temperature for $X_{Na} = 0.40$.

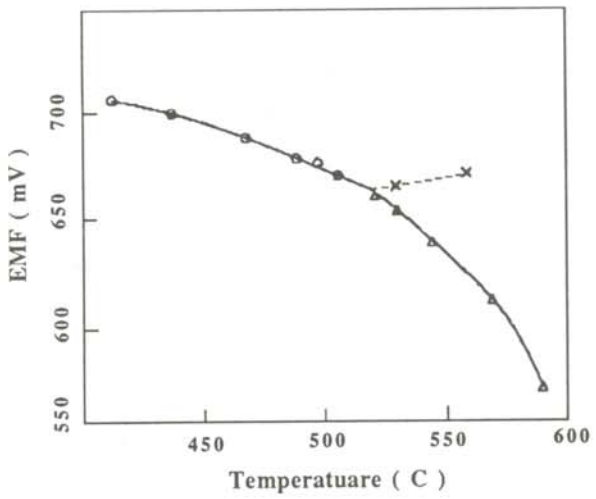

Figure 6
Liquidus Lines composed of points where the emf readings at any given temperature are independent of the working electrode compositions.

been titrated into the working electrode, the emf between the working electrode and the counter electrode bath with the titration circuit broken remained near 0.1 mV.

The liquidus lines plotted in Figure 6 are composed of points where the emf readings at any given temperature are independent of the composition of the working electrode. The two solid curves are reasonably certain. Their intersection determines the eutectic temperature. Two points, the dashed line in Figure 6, taken using the working electrode at 40 at% Na (which did not reach equilibrium) provide a clue to the third liquidus line. This line is very tentative. We determined the eutectic temperature to be 519.6 C. Previous results [8] placed the eutectic at approximately 508.6 C, due to higher emf readings on the low temperature liquidus line.

The intersection of the liquidus lines of Figure 6 combined with the plots of emf vs. T of Figures 3-5 determine the phase diagram and the eutectic composition. With this procedure, the results of which are shown in Figure 7, one finds that Na-As reaches the liquidus line at 555 C for 45.31 at% Na, at 532 C for 42 at% Na and at 522 for 40 at% Na. Figure 7 also shows that the eutectic composition must be just under 40 at%Na.

The resulting partial phase diagram appears in Figure 8. The three points fit the quadratic equation:

$$T = 938.5 - 2509.2\ X_{Na} + 3669.8\ X^2_{Na}$$

where T is the temperature and X_{Na} is the atomic fraction of Na. The solutions to this equation

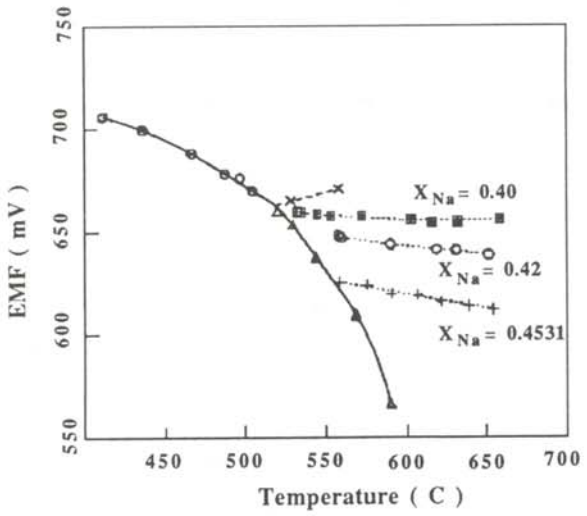

Figure 7
Complete plot of emf vs. temperataure for various compositions of the Na-As alloy.

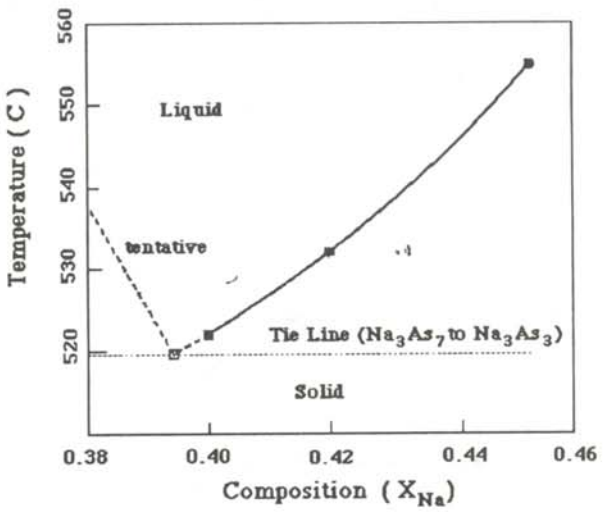

Figure 8
Partial phase diagram of Na-As.

when T = 519.6 C are 0.2897 and 0.3941. Since the eutectic composition, as seen in Figure 8, must be just below 40 at% Na, the latter solution must be the correct atom fraction of Na at the eutectic.

ACKNOWLEDGMENTS

The author especially thanks Dr. Marie-Louise Saboungi for her guidance and patience in the lab. Thanks also go to Dr. Anthony Petric for his experimental expertise, to Dr. Milton Blander for his interest in our work and to Elaine Estand and Dr. Romesh Kumar for their help in creating the computer file for this report.

REFERENCES

* This work was performed at Argonne National Laboratory while the author was a participant in the Summer 1990 Student Research Program.

1. E. Zintl, J. Goubeau and W. Dullenkopf, Z. physik. Chem., A154, 1931, pp. 32-33.

2. R. P. Elliott, Constitution of Binary Alloys: First Supplement, McGraw-Hill Book Co., New York, 1965, p. 74.

3. M. Hansen, Constitution of Binary Alloys, McGraw-Hill Book Co., New York, 1958, p. 1002.

4. Ibid., pp. 321-322.

5. F. W. Dorn, W. Klemm and S. Lohnmeyher, Z. Anorg. Allgem. Chem., 309, 1961, pp. 204-209.

6. C.H. Mathewson, Z. Anorg. Allgem. Chem., 50, 1906, pp. 187-192.

7. C.E. Johnson and A.K. Fischer, J. Less Common Metals, 20, 1970, pp. 339-344.

8. A. Petric, unpublished data.

9. E. Zintl and W. Dullenkopf, Z. physik. Chem., B16, 1932, pp. 183-194.

10. L.S. Darken, Trans. AIME, 239, 1967, p. 80.

11. A.B. Bhatia and D.E. Thorton, Phys. Rev. B, 2, 1970, p. 3004.

FACULTY SPONSORS

Dr. Marie-Louise Saboungi
Dr. Anthony Petric
Chemical Technology Division
Argonne National Laboratory
9700 South Cass Avenue
Argonne, IL 60439-4837
708-972-4341

The Journal of Undergraduate Research in Physics

The Journal of Undergraduate Research in Physics is the journal of Sigma Pi Sigma and the Society of Physics Students. It is published by the Physics Department of Guilford College, Greensboro NC. Inquiries about the journal should be sent to the editorial office.

The Journal of Undergraduate Research in Physics

Editorial Office -

The Journal of Undergraduate Research in Physics
Physics Department
Guilford College
Greensboro, NC 27410
919-292-5511 (voice)
919-854-3606 (FAX)

Editor -

Dr. Rexford E. Adelberger
Professor of Physics
Department of Physics
Guilford College
Greensboro, NC 27410

The Society of Physics Students

National Office -

Dr. Donald Kirwin, Executive Director
Dr. Edwin Goldin, Associate Director
Society of Physics Students
American Institute of Physics
1825 Connecticut Avenue, N.W.
Suite 213
Washington, DC 20009
202-232-6688

President of the Soceity -

Dr. Gary Agin
Department of Physics
Michigan Technological University
Houghton, MI 49931

POST USE TEXTBOOK REVIEW

Classical Mechanics

A. Douglas Davis
Harcourt Brace Jovanovich, Publishers, 1986.

Reviewed by:

Christy Beacham, Mark Whitehead,
Seth Snell and Lewis Adams Riley

Physics Department
Guilford College
Greensboro, NC 27410

We used this text in conjunction with regular lectures for a junior level Classical Mechanics class. Some of the sections that we covered include: basic one-dimensional motion, the harmonic motion, central forces, systems of particles, rigid bodies and Lagrangian Mechanics. Davis also expediently presents chapters on statics, fluid mechanics and special relativity.

Davis' writing style is engaging, clear and more lively than similar discussions found in Marion's [1] mechanics book. His style is conducive to his goal: to help students apply calculus to solve classical mechanics problems and to aid the student in understanding new ideas. Davis could fulfill this goal in a better way if three problems were solved.

First, if the students are supposed to learn how to use calculus effectively, the derivations for various ideas, such as the inverse square force, should include more steps. It seems as though Davis uses phrases like "with a little algebraic fidgeting" and "clearly" to save steps that are essential to grasping a basic understanding of calculus-based applications.

It would also be helpful if Davis used a more general approach in presenting the material. In some instances, such as the section on moment of inertia tensors, a special case is presented rather than a more generally applicable approach. The general approach might widen the range of problems the student could attack and would give the students more background which would make assimilating the specific approach easier.

Thirdly, there are several editing mistakes that seriously hinder understanding the material. Several minor editing mistakes like incorrect references to equations and incorrect units in the problems add up to make trying to understand the material more frustrating than it already is.

Seth, Mark and Lew are junior physics majors at Guilford College. Seth and Lew are pursuing minors in philosophy. Mark worked this semester as a teaching assistant in Stellar Astronomy, a popular way for the Guilford students to meet their lab science requirement. Christy, a senior, started out majoring in chemistry and switched to physics as an upper class student. She is currently applying to graduate school in medical physics.

Speaking of problems, Davis has compiled an interesting and creative set of questions at the end of each section. Instead of asking questions that are similar to the examples given throughout each section, the questions are taken out of context. For example, after presenting Rutherford scattering and central forces, there is a question concerning a star moving through stellar debris that asks to show that all the debris ahead of the star inside a certain radius will collide with the star. There are several problems like this one that force the students to look at the material in a different setting than the way the ideas are presented. This is an excellent way to practice creative problem solving.

The text also includes helpful appendices that contain information concerning calculus, multiple integrals and a matrix review. We were pleasantly surprised to discover brief sections on numerical methods for BASIC and Pascal. The numerical methods are designed to introduce basic ways of solving mechanics problems using the computer and could be applied to several of the sections throughout the book. In fact, Davis gives several interesting problems throughout the book that must be solved numerically. Moreover, Davis gives simple and functional algorithms that are easily understood even if the students have little or no programming background.

We felt that the text's greatest strengths lie in the stimulating problems, the sections on numerical methods and the clear writing style. Although the editing mistakes are frustrating, they will surely be expunged in later editions. We wholeheartedly recommend this text as an excellent source of problems and a basic reference to be accompanied by more detailed lectures.

1) J.B. Marion, Classical Dynamics of Particles and Systems, Academic Press.